GROUND DISPLACEMENTS ON AITIK TAILINGS DAMS USING SAR INTERFEROMETRY

Final Report

Authors: Line Rouyet, Tom Rune Lauknes and Corine Davids

norut
NORTHERN RESEARCH INSTITUTE

PROJECT NAME: RESEM   **PROJECT NO.**: 602

CONTRACTING: Interreg Nord, Troms Fylkeskommune

AUTHORS: Line Rouyet, Tom Rune Lauknes and Corine Davids

TITLE: Ground displacements on Aitik tailings dams using SAR Interferometry

---

SUMMARY:

As part of the REmote SEnsing supporting surveillance and operation of Mines (RESEM) project, we performed a preliminary study about the use of Synthetic Aperture Radar Interferometry (InSAR) for documenting ground displacements on tailings dams (Aitik copper mine, Sweden). The Stacking and SBAS methods have been applied to map the spatial distribution of the ground displacements based on 2015–2017 TerraSAR-X and Sentinel-1 satellite data, as well as to retrieve time series between May and November 2017. The 2D InSAR method has been used to combine results from ascending and descending SAR geometries. The report summarized described the main findings of the InSAR analysis and discuss the potential and limitations of the technique for applications in in the mining sector.

Key words: Synthetic Aperture Radar (SAR), SAR Interferometry (InSAR), Ground Displacements, Tailings Dam Stability

Noter: -

UTGIVER: Norut, Postboks 6434, 9294 Tromsø, Norway

CONTENT

1 INTRODUCTION

REmote SEnsing supporting surveillance and operation of Mines (RESEM) is a project funded by Interreg Nord. As part of the work package 3 (Mining structures and operation processes), we investigated how satellite remote sensing can be used to help to monitor the stability of mining structures. Aitik open pit copper mine in Sweden was selected as a case study for testing the ability of Synthetic Aperture Radar Interferometry (InSAR) to document ground displacements on tailings dams. The report introduces quickly the principles of InSAR (*Section 2*) and describes the data used for the case study (*Section 3*). The results of the InSAR processing are presented in *Section 4* and the main findings are summarized in *Section 5*.

2 SAR INTERFEROMETRY

In active microwave remote sensing, electromagnetic waves are transmitted from an active sensor and the echoes scattered by the Earth's surface are then recorded and processed (*Figure 1, left*). Synthetic Aperture Radar (SAR) images are acquired when the satellite is flying along its ascending orbit (crossing the equator from South to North) or descending orbit (crossing the equator from North to South) (*Figure 1, right*). SAR Interferometry (InSAR) is a technique that analyses the phase shift of the electromagnetic wave between two SAR acquisitions. By combining images taken at different times, the phase shifts can be used to document at mm-level how the ground surface moves along the measuring line-of-sight (LOS) of the radar. Each pair of SAR images used for the calculation of the phase shifts is called "interferogram". Several interfograms are combined to document the averaged ground velocity and the evolution of the displacements during the measurement period.
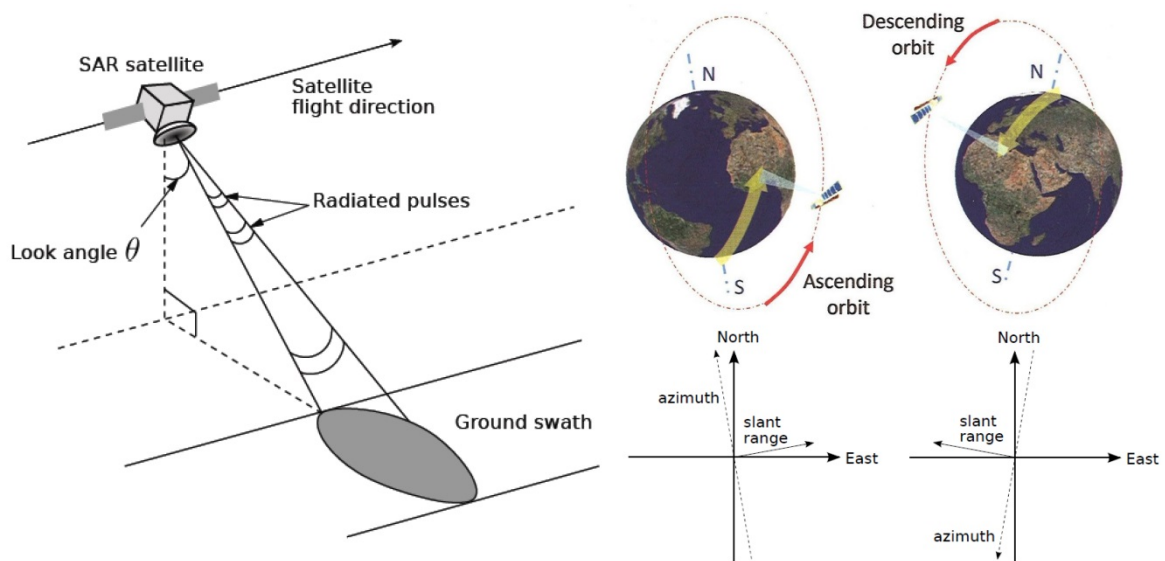
Figure 1: Left: Simplified geometry of a Synthetic Aperture Radar (SAR) system. InSAR detects distance changes between the SAR satellite and the ground, i.e. LOS displacements. From Lauknes, 2010. Right: Geometry of ascending and descending satellite orbits. Modified from Ferretti, 2014; Lauknes, 2010.

The results were obtained using the Norut GSAR InSAR software (Larsen et al., 2005) using two different methods: Stacking method (mean velocity calculation) which provides only information about the spatial distribution of the displacements (Sandwell & Price, 1998); and Small BAseline Subset (SBAS) method to retrieve time series (Berardino et al., 2002). Results presented on the maps in *Section 4* are expressed in averaged annual mean velocity extrapolated from the snow-free period. Time series document the temporal evolution of the displacement during ca. 6 months. Reliable InSAR measurements cannot be retrieved on areas affected by severe changes of ground properties, due e.g. to vegetation, wetness or too large movements that lead to phase decorrelation, or loss of signal ("coherence"). Pixels with poor stability quality or low coherence are thus masked out during the processing. The threshold is based on the coherence of a chosen percent of all considered interferograms.

InSAR measurements are one-dimensional and correspond to distance changes between the ground and the sensor, i.e. displacements along the line-of-sight (LOS). For an ascending SAR geometry, an area affected by horizontal westward displacements corresponds to negative InSAR values (decrease of sensor-ground distance, blue on maps). For a descending SAR geometry, the same area corresponds to positive InSAR values (increase of sensor-ground distance, yellow to red on maps). By combining results from both geometries, two-dimensional information can be retrieved (2D InSAR method, Eriksen et al., 2017).

3 DATA AND STUDY SITE

In this study, we used four SAR datasets acquired during the summer seasons 2015, 2016 and 2017: 21 TerraSAR-X (TSX) images in ascending geometry, 24 TSX images in descending geometry, 48 Sentinel-1 (S1) images in ascending geometry, and 53 Sentinel-1 (S1) images in descending geometry. Characteristics of SAR data are summarized in *Table 1*. The parameters used for InSAR processing are shown in *Table 2* (in attachment).

Table 1: Characteristics of SAR datasets

| SAR sensor	SAR mode / geometry	Frequency band (wavelength)	Revisit time	Spatial resolution (original / final)	Number of scenes	Time period	LOS (azimuth / incidence angle)
TSX	StripMap / ascending	X (λ: 3.1 cm)	11 days	2.1x1.9m 10x10 m	21	14.07.2016–16.09.2017	78º / 41.4º
TSX	StripMap / descending			2.1x1.9m 10x10 m	24	05.06.2016–13.10.2017	285º / 30.1º
S1	IWS* / ascending	C (λ: 5.55 cm)	6(12)** days	5x20m / 40x40 m	48	13.05.2015–04.11.2017	78º / 38.6º
S1	IWS* / descending			5x20m / 40x40 m	53	09.06.2015–01.11.2017	285º / 30.4º

* IWS: Interferometric Wide Swath mode, ** 12 days until September 2016, 6 days after

In Aitik, several mining structures have been investigated using InSAR (*Figure 2*). The main focus of this study is placed on the tailings dams in the western part of the mining area (red line, *Figure 2*). The InSAR displacements are calibrated against an area assumed to be stable south from the main dam (red star, *Figure* 2). The two SAR acquisition geometries are necessary to document the different components of the ground displacements on the dams. *Figure 3* shows as example the measuring angles provided by TSX satellite in ascending and descending geometries.
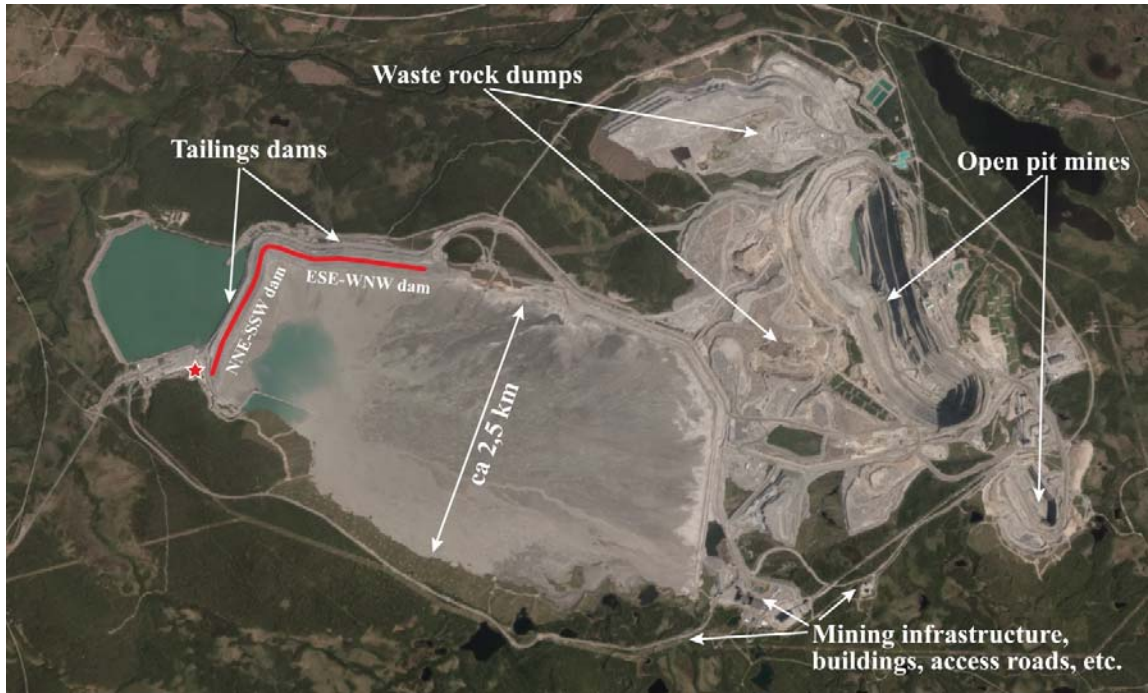
Figure 2: Location map: Aitik copper mine and elements under study. Red line: Main tailings dams (focus of the study). Red star: InSAR calibration area.
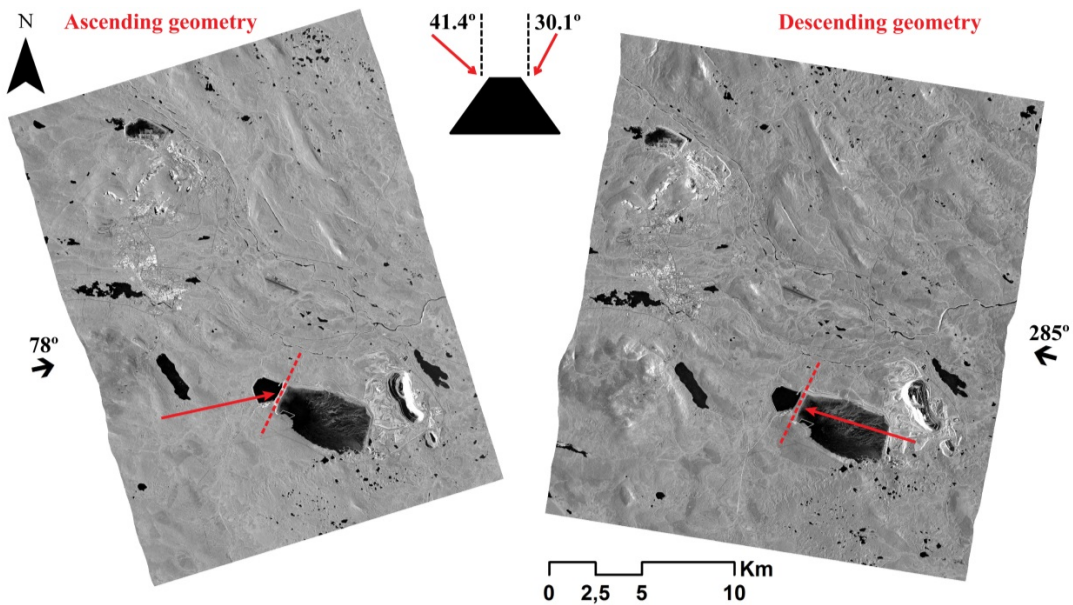

Figure 3: Mean SAR intensity images from TSX in ascending and descending geometries. Arrows indicate the LOS orientation. The inset shows the LOS on a simplified cross-section of the NNE-SSW tailings dam.
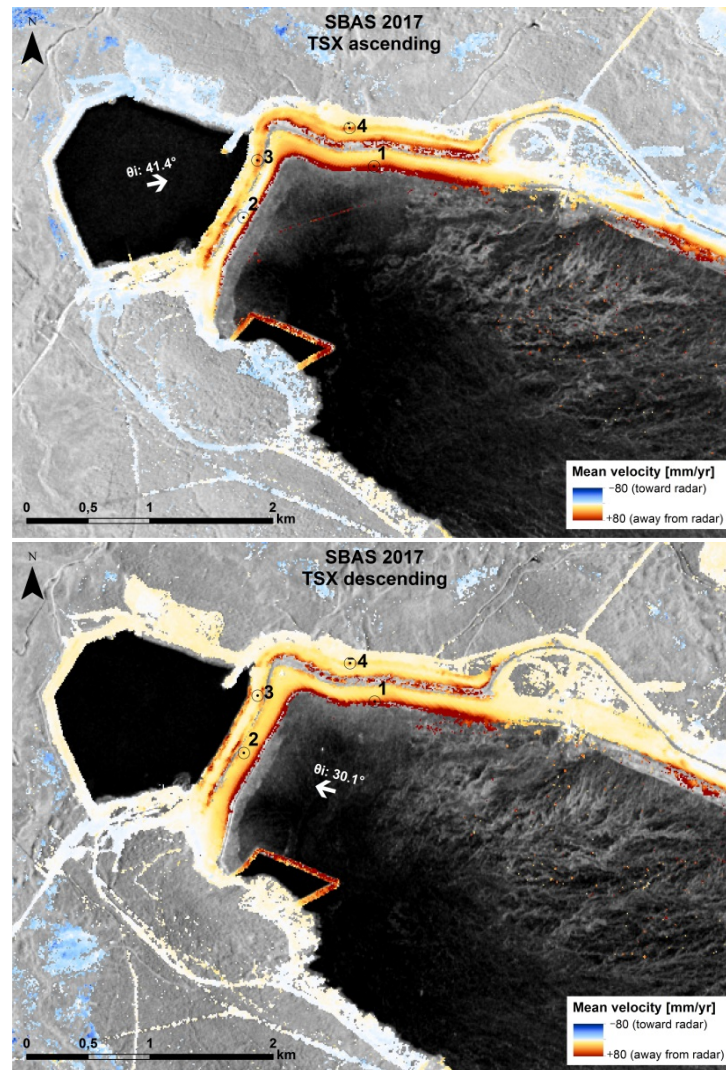
4 RESULTS

By applying the Stacking method based on interferograms from all available summer seasons (2016–2017 for TSX, 2015–2017 for S1), the spatial distribution of ground displacements in Aitik can be mapped. In *Figure 4*, the results for TSX and S1 in descending geometries are shown and compared. Similar results for the ascending geometries are available in attachment (*Figure 13–14*). Pixels in gray-black correspond to areas that have been masked out during the processing (low coherence), where InSAR is not able to retrieve reliable information due to wetness (e.g. in tailing area, on lakes), too fast changes (e.g. in the open pits or on the dams where severe construction work took place) or vegetation (surrounding areas). The pixels outside the main mining sector can be affected by errors due to the spatial discontinuity of InSAR coherent patches. Focusing on the tailings dams, we can see that downward and/or westward displacements are detected (yellow-red pixels in *Figure 4*). Both TSX and S1 maps highlight overall similar patterns. S1 results have a lower spatial resolution (*Figure 4*, lower), which explains that small and fast moving areas on the dams are not clearly detected.
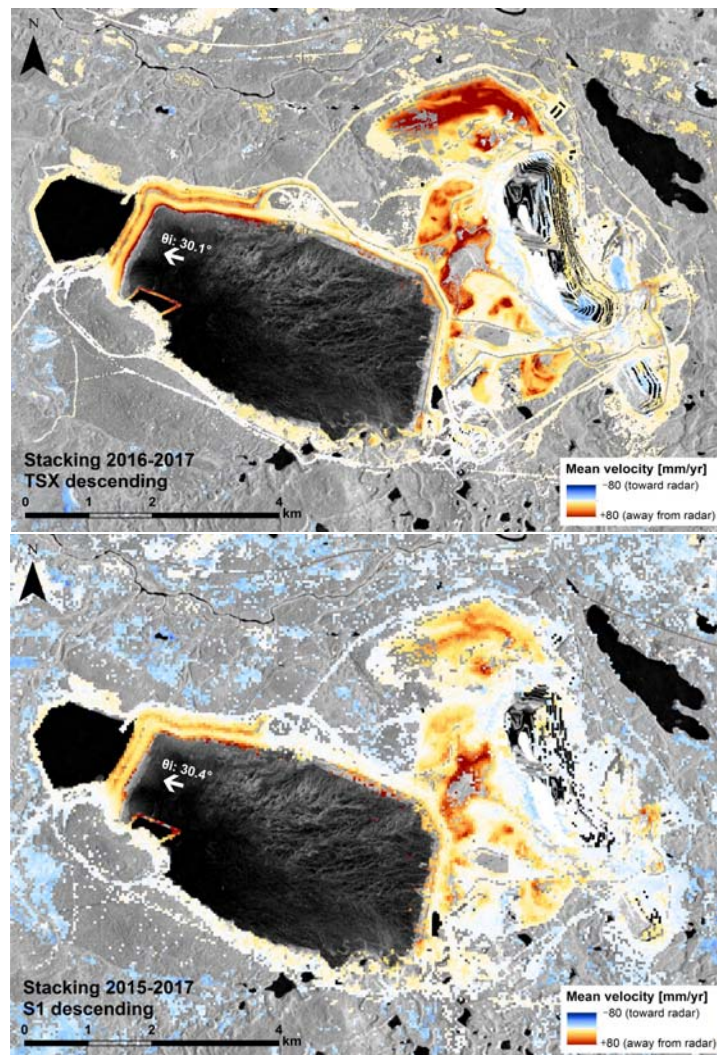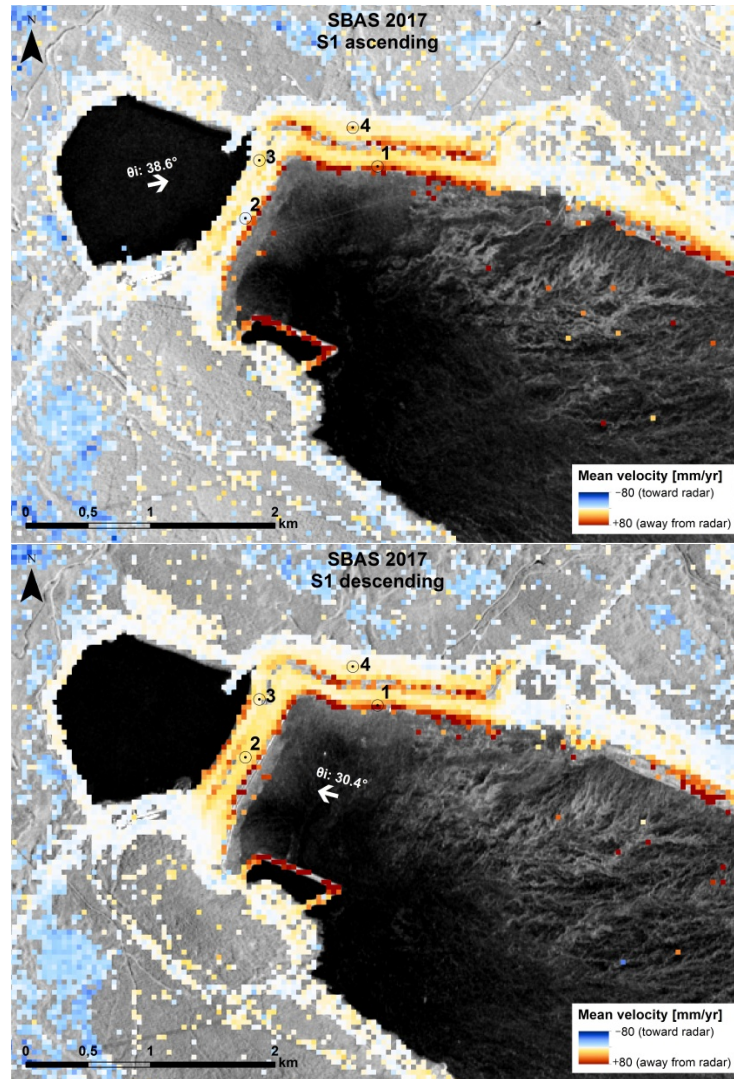

Figure 4: Mean velocity maps based on Stacking results in descending geometry. Upper: TSX 2016–2017. Lower: S1 2015–2017. Background: Mean intensity image. White arrow: Line-of-sight orientation.

By applying the SBAS method based on interferograms from 2017 summer season only, we can also map the extrapolated annual mean velocity (*Figure 5*: TSX results for both geometries, *Figure 6*: S1 results for both geometries). In addition, it is possible to retrieve time series for each pixel where InSAR is able to measure ground displacements.

Spatially, the SBAS method highlights in general the same patterns as the Stacking method. On the NNE-SSW dam, the difference between the results from the ascending and descending geometries gives information about the orientation of movement. Negative values (light blue) are detected in the middle/upper part of the structure on TSX/S1 ascending results (*Figures 5–6*, upper), while the same area appears in yellow-red colors (positive values) in descending results (*Figures 5–6*, lower). It indicates that this part of the structure is mainly affected by horizontal displacement toward the West, leading to a decrease of the sensor-ground distance for the ascending geometry and an increase for the descending geometry. At other locations, dark red areas on results from both ascending and descending geometries indicate large downward displacements (subsidence).


Figure 5: TSX mean velocity maps based on SBAS results in 2017. Upper: Ascending geometry. Lower: Descending geometry. Background: Mean intensity image. White arrows: Line-of-sight orientations. Black circles: Location of time series shown in *Figures 7–8* and *Figures 17–18*.

6

Figure 6: S1 mean velocity maps based on SBAS results in 2017. Upper: Ascending geometry. Lower: Descending geometry. Background: Mean intensity image. White arrows: Line-of-sight orientations. Black circles: Location of time series shown in *Figures 7–8* and *Figures 17–18*.

Temporally, time series can be plotted and document the evolution of the ground displacement during the measurement period (May–November 2017). Four examples have been extracted and are shown in *Figures 7–8* (and *Figures 17–18* in attachment). The values are relative to the first acquisition of each dataset processed individually. In *Figures 7–8* (and *Figures 17–18*) however, in order to provide a better comparison, TSX time series, that are starting slightly later in the season, have been shifted according to the values measured by S1 for each geometry. TSX and S1 results show overall similar patterns. Some mismatches can be explained by the intrinsic differences of sensor/dataset properties (spatial resolution, revisit time, radar frequency affecting the sensitivity to decorrelation, etc.). Again, by jointly analysing the results from ascending and descending geometries, we can tell more about the orientation of the deformation. The overall similar values in both geometries shown in *Figure 7* indicate that the location 1 is mainly affected by subsidence, while the opposite trends measured by the two geometries and shown in *Figure 8* indicate that the horizontal component is significant at location 2.

7
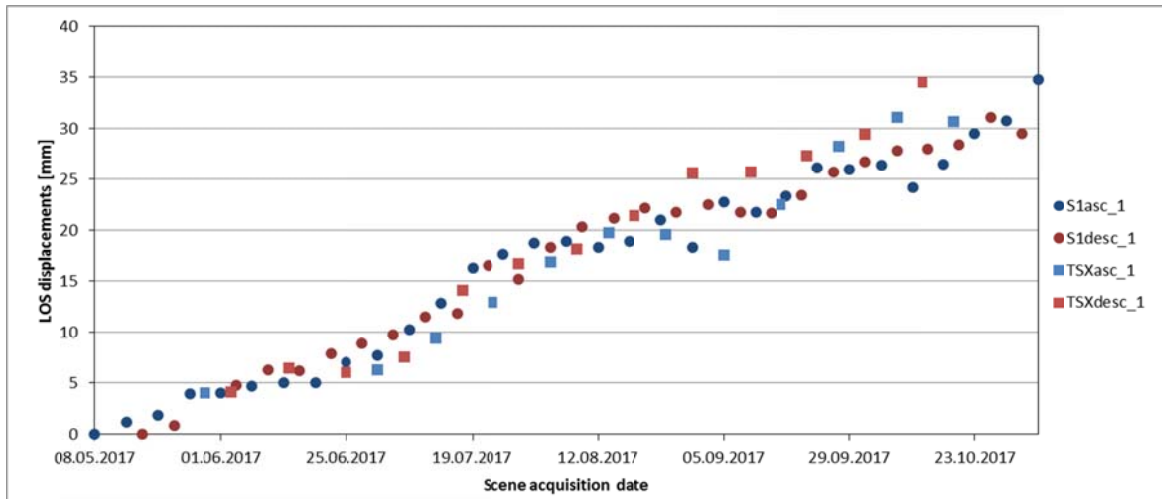
Figure 7: Example of SBAS time series at the location 1 for TSX and S1 in ascending and descending geometries. Location: Black circle 1 in *Figures 5–6*.
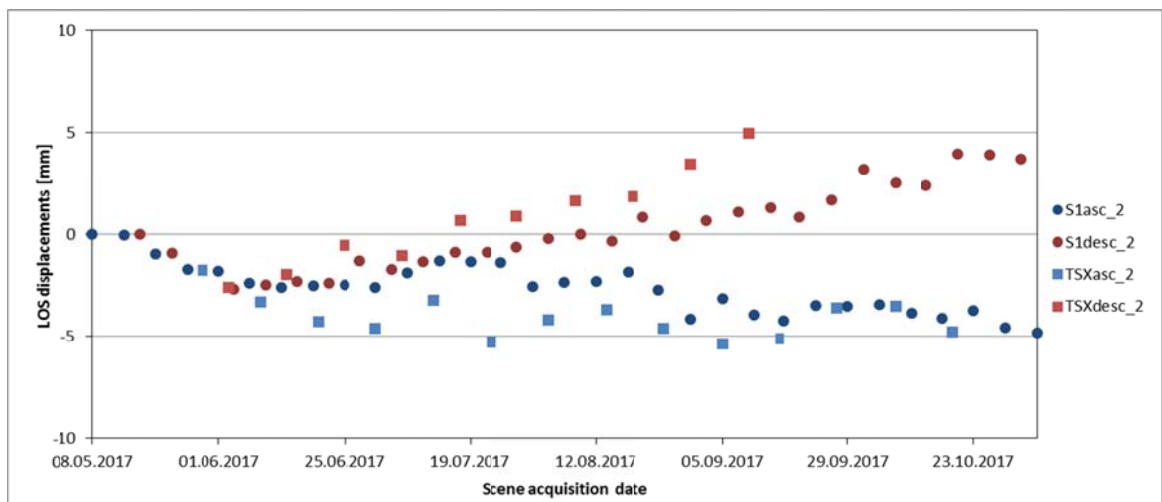

Figure 8: Example of SBAS time series at the location 2 for TSX and S1 in ascending and descending geometries. Location: Black circle 2 in *Figures 5–6*.

In order to better exploit the complementarity of the two geometries, it is possible to combine both results, calculate 2D vectors and decompose the mean velocity values into vertical and E-W horizontal components. Based on Stacking results, 2D InSAR method is thus applied both for TSX and S1 results. The maps of the amplitude of the 2D vectors are available in attachment (*Figures 15–16*). Vertical and horizontal components maps are separately shown in *Figures 9–10*.

On the dams, TSX and S1 results are consistent and show that the structures are affected by a combination of vertical and horizontal displacements. The effect of the different spatial resolution is however again clearly visible. Downward movements are detected on most of the dam surfaces with variable amplitudes. The highest velocity values are located in the inner parts of the dams. Horizontal displacements toward the East or the West are detected, depending on the location along the structure. The NNE-SSW dam is mainly affected by westward deformation. Combined with the detected vertical component, this corresponds to an expected downslope orientation of the displacements.

8

As the slope orientation gets inversed in the inner part, the horizontal component becomes logically eastward. On the ESE-WNW dam, it is more difficult to retrieve totally meaningful information due to the structure orientation unfavorable to InSAR LOS measurements. It is likely that significant parts of the real displacements have a N-S horizontal component that we cannot detect. However, as expected, horizontal E-W patterns show a slight eastward component in the outer part of the dam, and a westward component in the inner part.
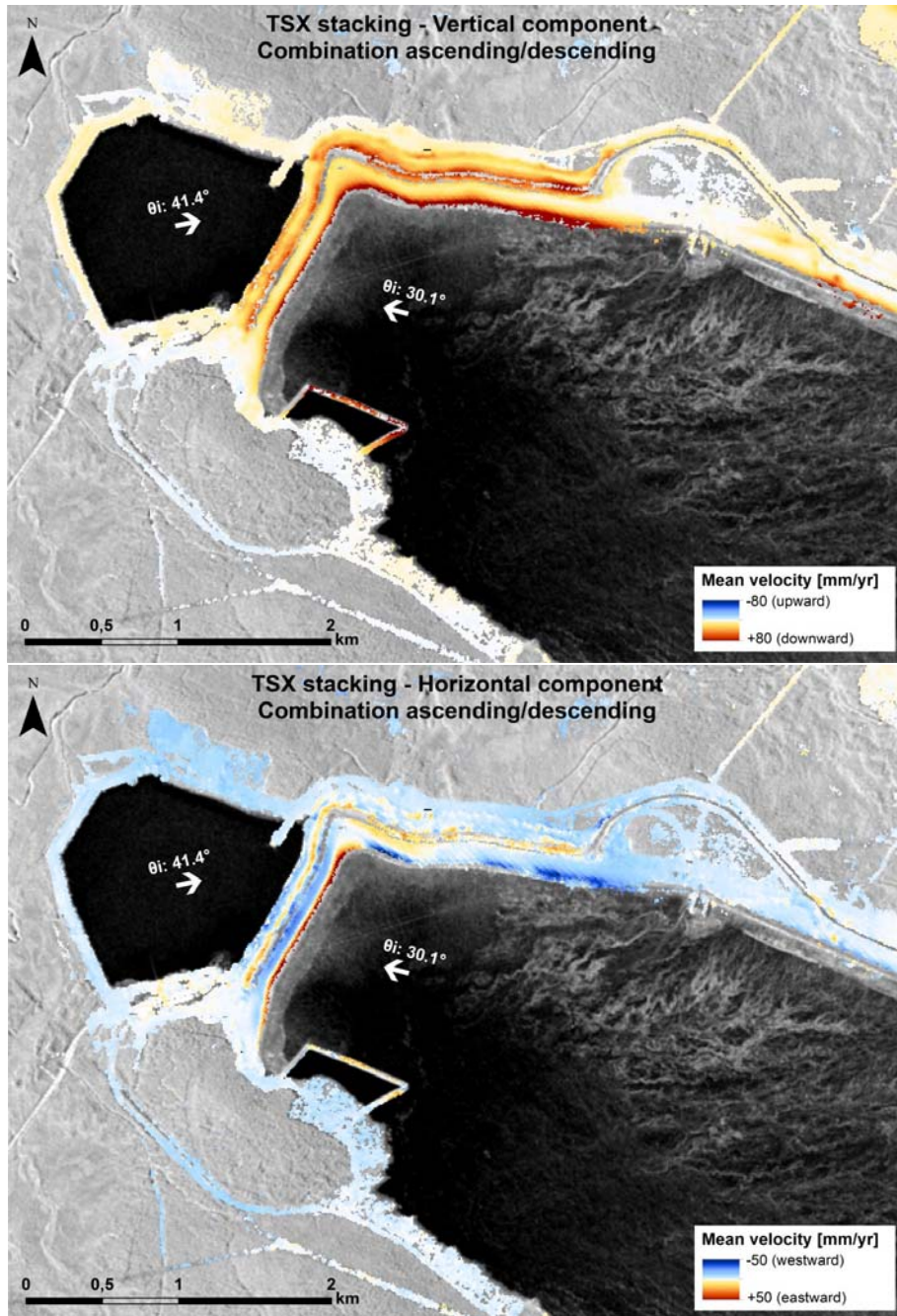
Figure 9: Decomposition of the vertical (upper) and the E-W horizontal (lower) components of the displacements based on 2D InSAR method (combination of TSX stacking in ascending/descending geometries). Background: Mean intensity image. White arrows: line-of-sight orientations.
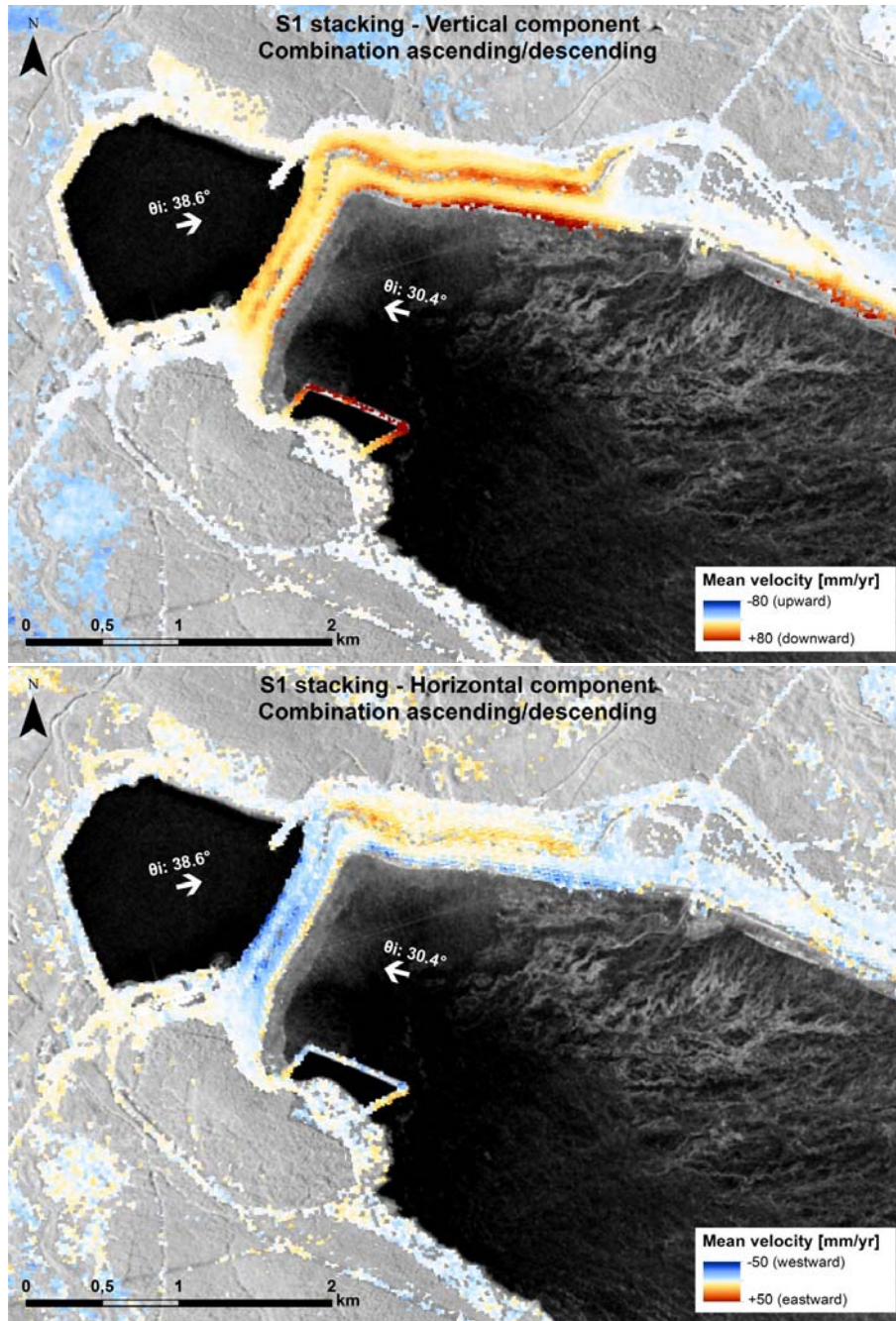
Figure 10: Decomposition of the vertical (upper) and the horizontal (lower) components of the displacements based on 2D InSAR method (combination of S1 stacking in ascending/descending geometries). Background: Mean intensity image. White arrows: line-of-sight orientations.

Vertical and horizontal InSAR results can visually be combined on a cross-section. *Figures 11–12* show the results for TSX and S1 along 62+316 profile *(location in Figure 19, left* in attachment*)*. With both sensors, the inversion of the movement direction following the slope orientation is visible, but large differences between TSX and S1 are also highlighted. Again it is important to stress the effect of the spatial resolution that for example can explain the lower S1 velocities detected in the middle of the WNW slope. In addition, it should be reminded that the measurement periods are not similar for both datasets (TSX: averaging of 2016–2017 seasons, S1: averaging of 2015–2017 seasons).

The profile crosses the location of a borehole where measurements have been performed using an inclinometer (blue square in *Figures 11–12*). The inclinometer recorded 9 mm of displacements between August and November 2017 (*Figure 19, right*, in attachment). Extrapolated to mean annual velocity, this corresponds to ca 27 mm. The order of magnitude sounds reasonable comparable to InSAR data. However, a direct comparison between the in-situ measurements and the InSAR results is unfortunately difficult to make, due to the difference in data properties. An inclinometer measures the horizontal deformation along a vertical profile into the ground, while InSAR provides information about the vertical and E-W horizontal movements at the ground surface.
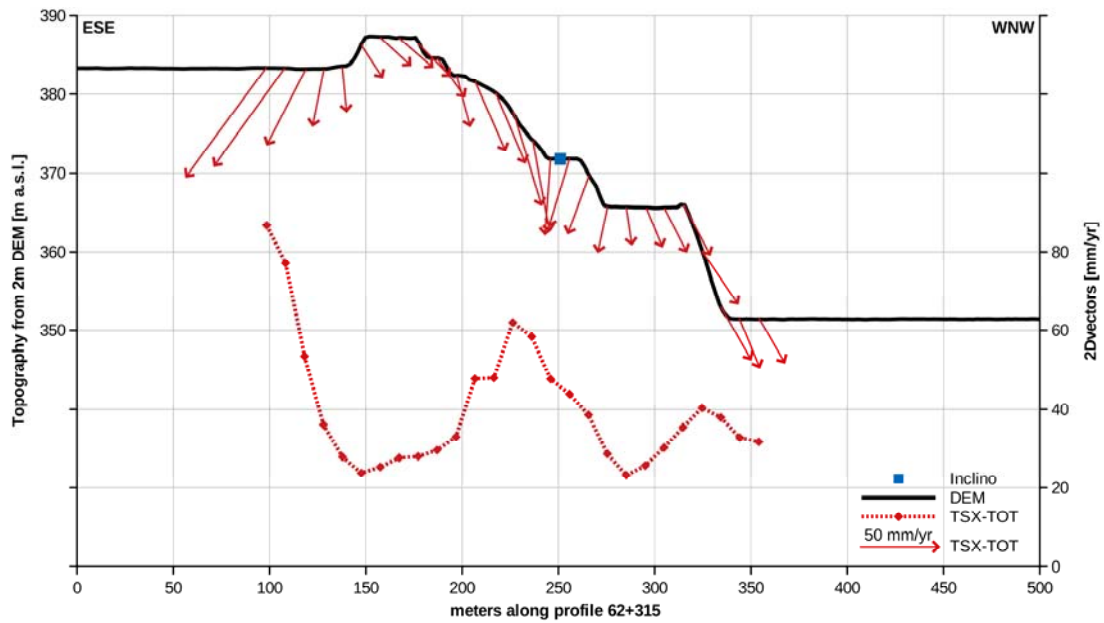
Figure 11: 2D vectors from combination of TSX Stacking results in ascending/descending geometries. Location of profile 62+315 in *Figure 19*.
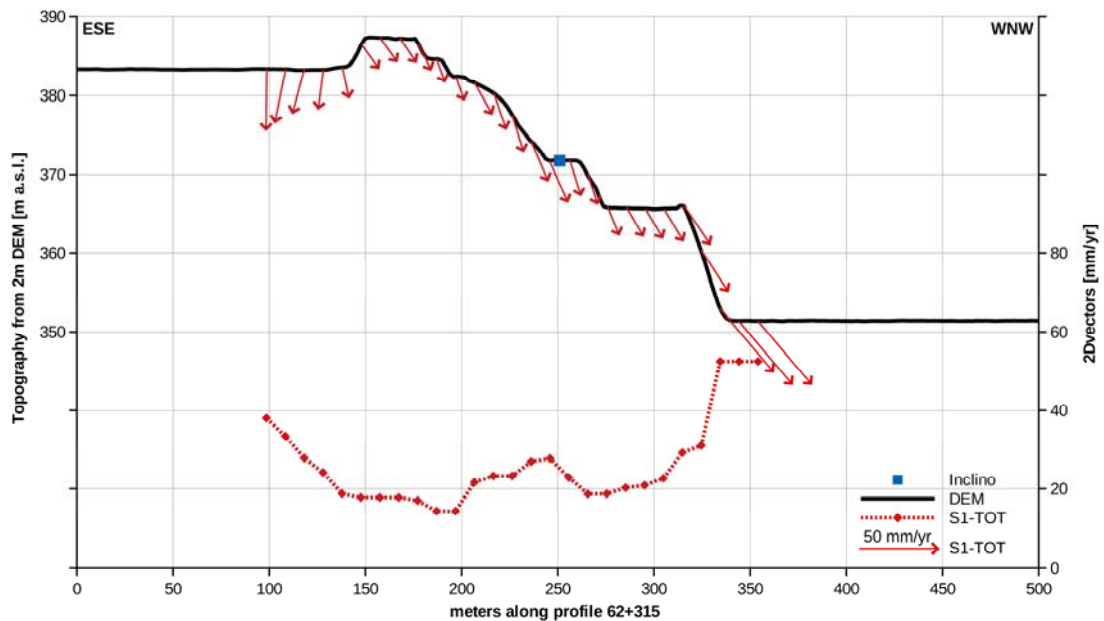
Figure 12: 2D vectors from combination of S1 Stacking results in ascending/descending geometries. Location of profile 62+315 in *Figure 19*.

5 CONCLUSION AND POTENTIAL

The results of the InSAR ground displacement measurements on Aitik tailings dams show that there is a potential of using SAR Interferometry to upscale the monitoring of dam stability. As other remote sensing techniques, InSAR has the advantage to provide measurements at a large scale without requiring a direct ground contact. This is of interest in a sector where the field conditions are challenging and where a good network of in-situ instrumentation is difficult and expensive to set up. In areas unaffected by decorrelation, InSAR provides accurate mm- to cm-scale measurements along the line-of-sight of the radar sensor, documenting the spatial distribution of the displacements (see Section 4, pp. 5–7) and the temporal evolution through the season (see Section 4, pp.7–8). In this study, we also showed that results from complementary SAR geometries can be combined to calculate 2D vectors and document further the kinematics of unstable areas (see Section 4, pp.8–11).

There are however several limitations that are important to keep in mind when looking at InSAR results. In Aitik, validation of the results could unfortunately not been performed due to fundamental differences of data properties (see Section 4, p.11). Further work and comparison with all potentially available in-situ information would be interesting in order to fully assess the reliability of the InSAR results. In active mining areas, the main problem is related to phase decorrelation, leading to signal loss in areas affected by wetness (issue in tailings area) and too large movements (issue on open pits and in areas subject to ongoing construction). The coherence-based filter applied to mask out the pixels affected by poor signal quality is currently the best way to discard decorrelated areas during the InSAR processing, but the selected areas may still include pixels with unreliable information if they are affected by a large disturbance occurring during a short period only (filter based on an averaged signal stability measure). An additional potential problem is the inaccuracy of the Digital Elevation Model (DEM) used for removing the topographical phase component. In a highly dynamic mining area, it is indeed likely that the topography changes significantly from one season to another. Finally, it must be reminded that even when applying the 2D InSAR method, the measurements do not give information about horizontal northward/southward components of displacement due to the E-W LOS orientations. For solving this issue, a terrestrial radar can be used to provide a third geometry with a complementary line-of-sight and potentially make possible the retrieval of 3D vectors. Based on the same principles as satellite InSAR, terrestrial radar interferometry has in addition the advantage to overcome some problems related to too fast movements due to minute-scale acquisitions.

Considering the advantages and limitations described above, there is a need for further research for applying InSAR in the mining sector. The European Commission Copernicus Sentinel-1 constellation is a game-changer that provides free data covering most of the world with a 6-days revisit time. Thanks to this data availability, operational monitoring based on SAR remote sensing becomes feasible and cost-effective.

6 REFERENCES

Berardino, P., Fornaro, G., Lanari, R. & Sansosti, E. 2002. A new algorithm for surface deformation monitoring based on small baseline differential SAR interferograms. *IEEE Transactions on Geoscience and Remote Sensing*, 40(11), 2375–2383. DOI:10.1109/TGRS.2002.803792.

Eriksen, H. Ø., Lauknes T. R., Larsen Y., Corner, G. D., Bergh, S. G., Dehls, J., Kierulf, H. P. 2017. Visualizing and interpreting surface displacement patterns on unstable slopes using multi-geometry satellite SAR interferometry (2D InSAR). *Remote Sensing of Environment*, 191, 297-312. DOI:10.1016/j.rse.2016.12.024.

Ferretti, A. 2014. *Satellite InSAR Data, Reservoir Monitoring from Space.* DB Houten, The Netherlands: EAGE Publications, Education Tour Series.

Larsen, Y., Engen, G., Lauknes, T. R., Malnes, E., & Høgda, K.-H. 2005. A generic differential SAR processing system, with applications to land subsidence and SWE retrieval. *Proc. ESA Fringe 2005, ESA ESRIN*, Frascati, Italy, November 28–December 2.

Lauknes, T. R. 2010. Rockslide mapping in Norway by means of interferometric SAR time series analysis. *Ph.D. Thesis*, University of Tromsø, Norway.

Sandwell, D.T. & Price, E.J. 1998. Phase gradient approach to stacking interferograms. *Journal of Geophysical Research*. 103(B12), 30183–30204. DOI:10.1029/1998JB900008.

7 ATTACHMENTS

Table 2: InSAR processing methods and parameters

|	Processing method	Multi-looking factor	Final ground resolution	Max. temporal baseline	Selected / discarded InSAR pairs	Coherence filter
TSX ascending	Mean velocity calculation (Stacking)	4x4	10x10 m	77d	74 / 11	0.25 in >50% pairs
TSX descending				77d	88 /17	0.25 in >50% pairs
S1 ascending		8x2	40x40 m	78d	273 / 235	0.40 in >50% pairs
S1 descending				78d	251 / 302	0.40 in >50% pairs
TSX 2017 ascending	Small Baseline Subset (SBAS) time series	4x4	10x10 m	77d	21 / 0	0.30 in >50% pairs
TSX 2017 descending				77d	54 / 9	0.25 in >50% pairs
S1 2017 ascending		8x2	40x40 m	78d	214 / 196	0.40 in >50% pairs
S1 2017 descending				78d	168 / 221	0.40 in >50% pairs
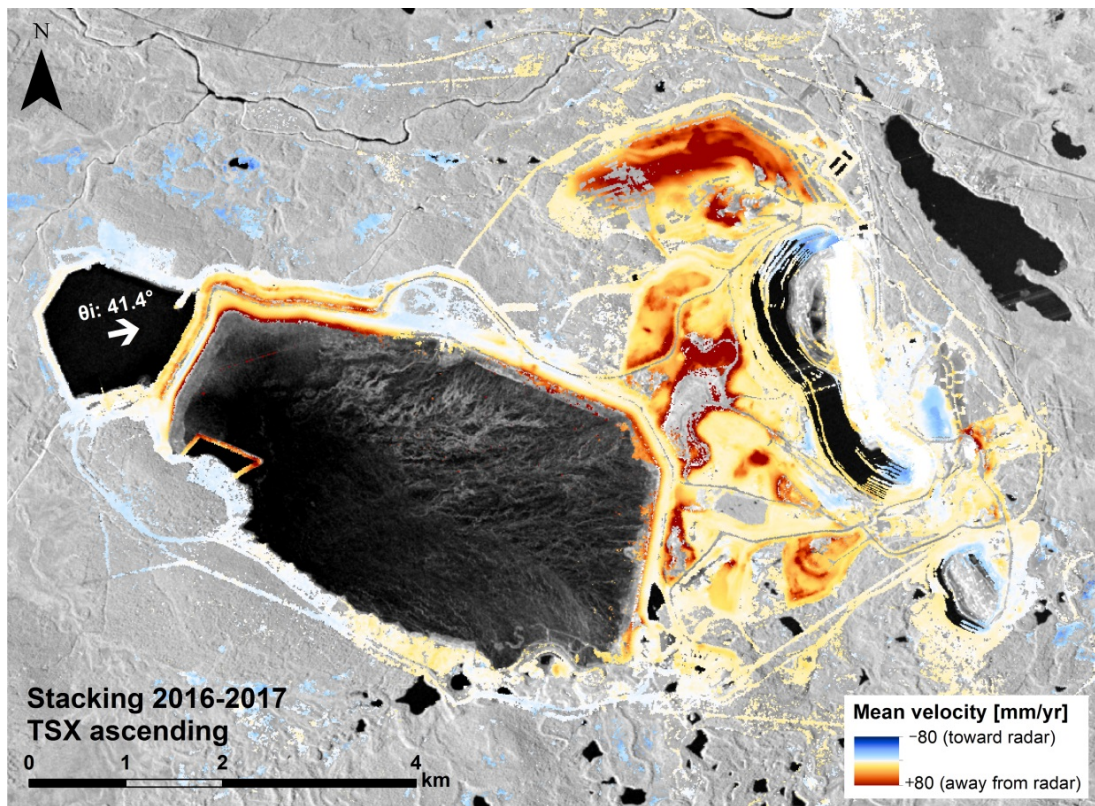
Figure 13: Mean velocity maps based on Stacking results based on TSX 2016-2017 (ascending geometry). Background: Mean intensity image. White arrow: Line-of-sight orientation.
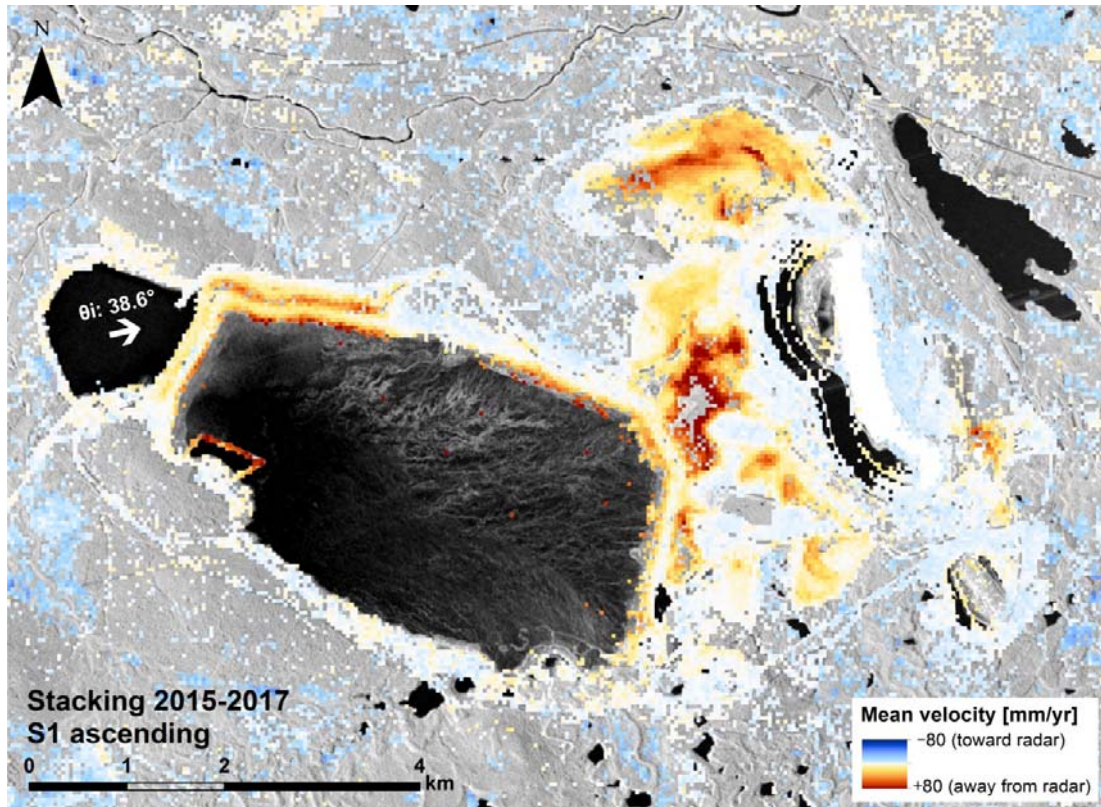
Figure 14: Mean velocity maps based on Stacking results based on S1 2015-2017 (ascending geometry). Background: Mean intensity image. White arrow: Line-of-sight orientation.
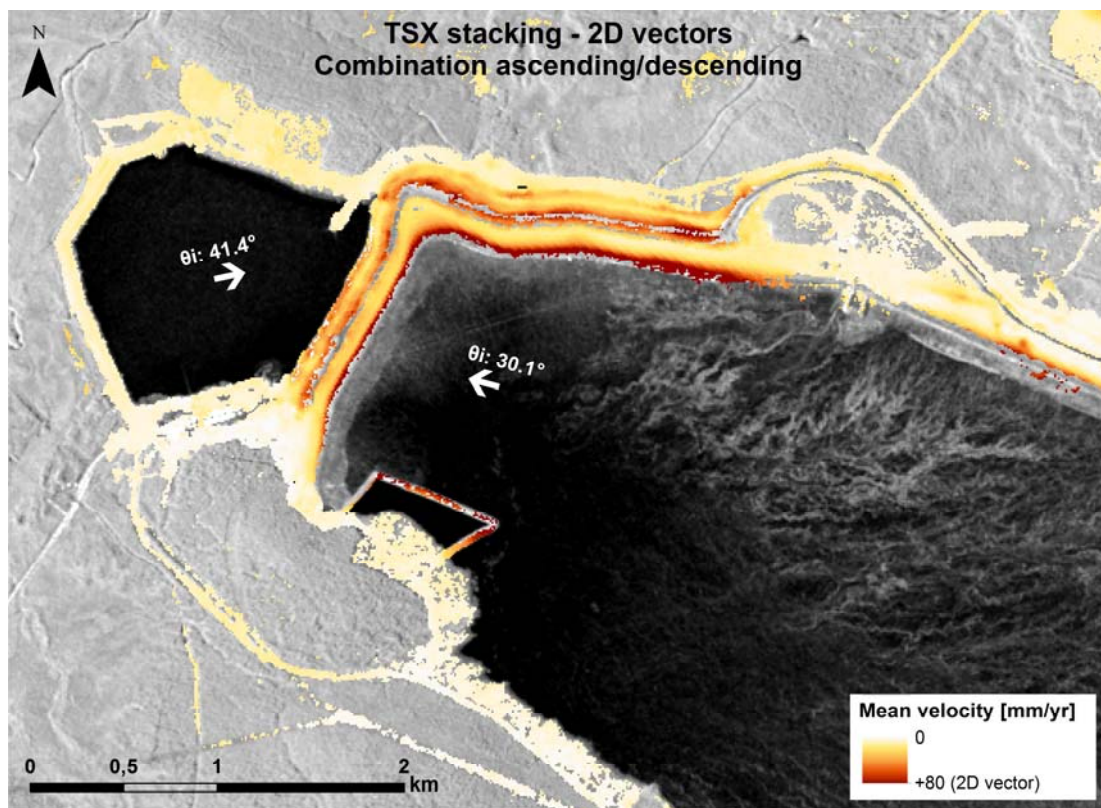

Figure 15: Amplitude of 2D vectors from 2D InSAR method (combination of TSX stacking in ascending/descending geometries). Background: Mean intensity image. White arrows: Line-of-sight orientations.
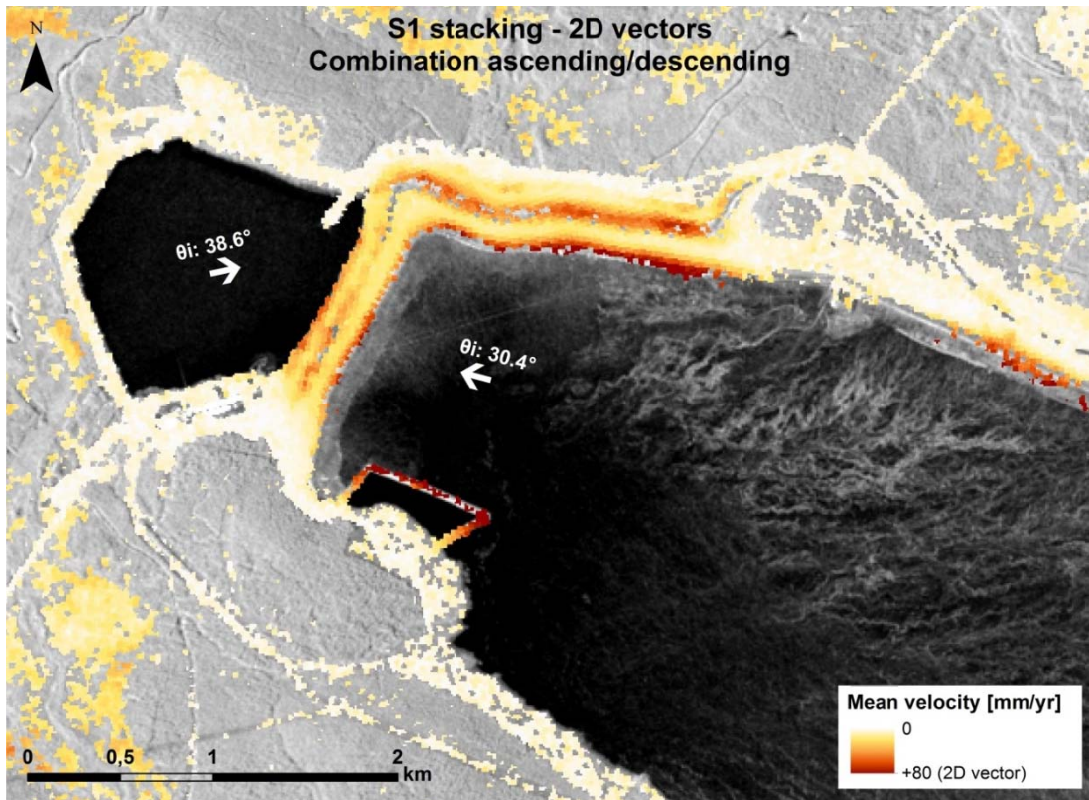
Figure 16: Amplitude of 2D vectors from 2D InSAR method (combination of S1 stacking in ascending/descending geometries). Background: Mean intensity image. White arrows: line-of-sight orientations.
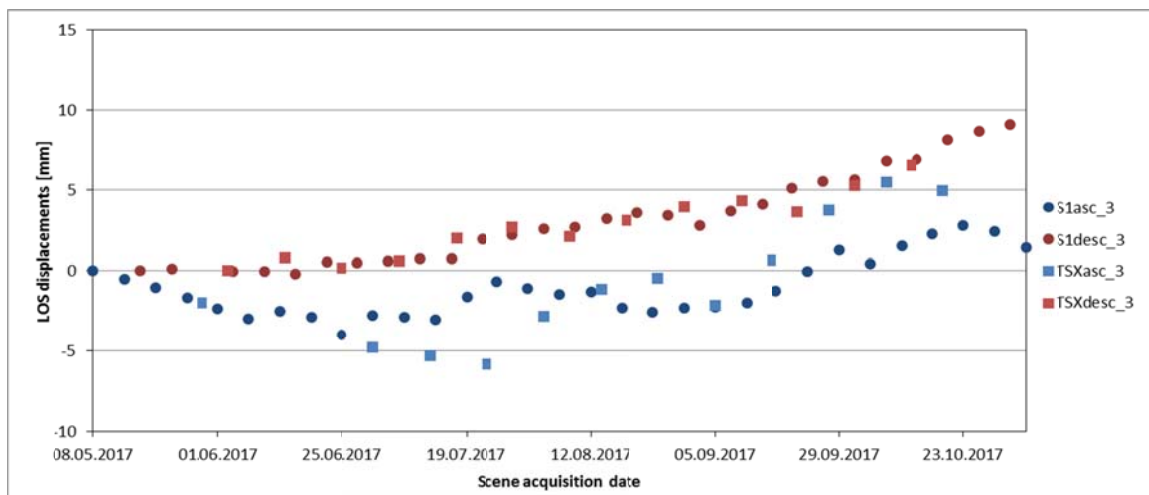
Figure 17: Example of SBAS time series at the location 4 for TSX and S1 in ascending and descending geometries. Location: Black circle 4 in *Figures 5–6*.
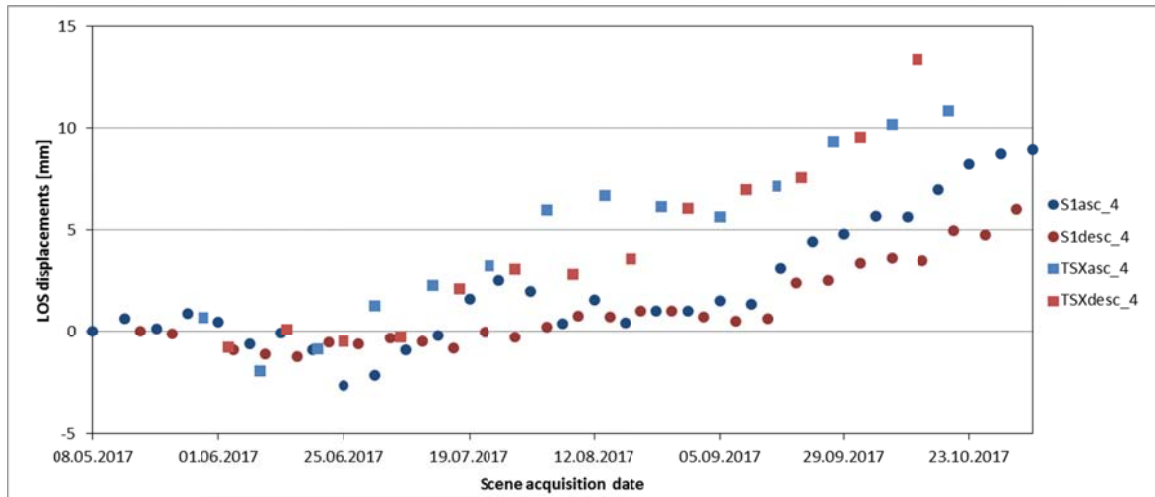
Figure 18: Example of SBAS time series at the location 3 for TSX and S1 in ascending and descending geometries. Location: Black circle 3 in *Figures 5−6*.
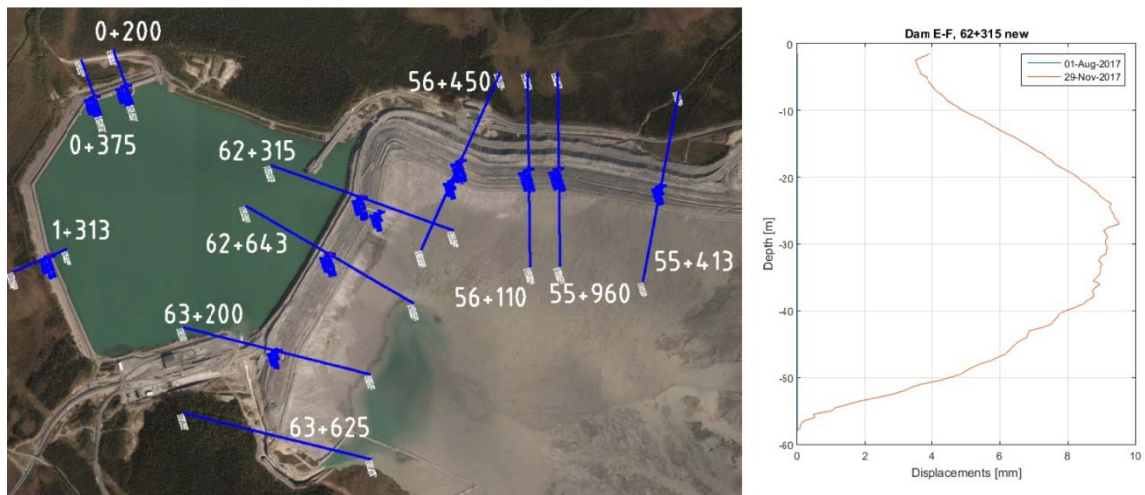
Figure 19: Left: Profiles and location of inclinometer instrumentation in Aitik. Profile 62+315 corresponds to the cross-section shown in *Figures 11−12*. Right: August to November 2017 displacements measured by inclinometer in borehole 62+315.